Int. J. Nano Dimens., 14 (1): 73-90, Winter 2023

ORIGINAL ARTICLE

Green synthesis of magnetite nanoparticles using *Catha edulis* plant leaf extract for removal of hexavalent Chromium from aqueous solution

Gudisa Hailu Chala, Tegene Desalegn Zeleke*

Department of Applied Chemistry, School of Applied Natural Science, Adama Science and Technology University, Adama, Ethiopia

Received 08 August 2022; revised 07 October 2022; accepted 14 October 2022; available online 19 October 2022

Abstract

In this study, we report the synthesis of magnetite (Fe_3O_4) nanoparticles using Catha Edulis plant leaf extract as bioreducing agents and investigation of its efficiency as an adsorbent for hexavalent chromium Cr(VI) removal from aqueous solutions. The synthesized NPs were characterized using X-ray diffraction (XRD) spectroscopy, Fourier Transforms Infrared (FTIR) spectroscopy, Scanning Electron Microscopy (SEM), Ultraviolet-visible (UV-Vis) spectroscopy, and thermal analysis (TGA-DTA). The XRD result revealed that the phase structure of Fe_3O_4 NPs was cubic face-centered with crystallite sizes of 12.1 nm, 14 nm, and 9 nm for metal to plant extract ratios of 1 : 1, 2 : 1, and 1 : 2 respectively. UV-Vis DRS analysis confirmed band gap energy of synthesized NPs was in the range 2.0-2.5 eV. Batch adsorption experiments were carried out to evaluate the effect of different parameters such as pH (3-10), adsorbent dose (250mg/L – 1250mg/L), initial concentration of adsorbate (20mg/L - 60mg/L), and contact time (30-120 min) on adsorption efficiency of the NPs at room temperature. The study revealed that the synthesized magnetite adsorbent exhibited Cr (VI) removal efficiency of about 98.6% at optimized conditions of adsorbent dose of 1000 mg/L, pH 5, initial concentration of Cr(VI) 20 mg/L, and contact time of 60 min. The experimental data were best fitted to the Freundlich adsorption isotherm model ($R^2 = 0.98341$). Moreover, the mechanism of adsorption was in good agreement with pseudo 2nd order kinetics ($R^2 = 0.98188$). The results suggested that the biosynthesized Fe_3O_4 nanoparticles have the potential for the removal of hexavalent chromium ions from aqueous solutions.

Keywords: *Adsorption Isotherm; Antibacterial activity; Catha Edulis; Green Synthesis; Magnetite NPs.*

How to cite this article

Hailu Chala G., Desalegn Zeleke T. Green synthesis of magnetite nanoparticles using Catha edulis plant leaf extract for removal of hexavalent Chromium from aqueous solution. Int. J. Nano Dimens., 2023; 14(1): 73-90.

INTRODUCTION

Heavy metal ions in aquatic environments are serious pollution problems for living organisms and public health. Heavy metals are non-biodegradable and tend to bioaccumulate. Hexavalent chromium ion is a one of the industrial pollutants posing serious ecosystem threats. The strong oxidizing properties of Cr (VI) trigger toxic effects on biological systems. Chromium could be released to the environment from leather tanning, metal processing, electroplating, pigment synthesis, dying, wood protection, electrical and electronic equipment industrial processes [1]. Inhalation and retention of chromium (VI) containing material can cause developmental issues, damage to the skin, respiratory, reproductive, and digestive systems, and cancer. Cr (VI) is much more toxic than Cr(III) because of its greater ability to enter cells and its strong oxidation potential. Once inside cells, Cr(VI) is reduced and produces free radicals, Cr(V), Cr(IV), and eventually Cr(III), which are believed to be responsible for toxic and carcinogenic effects [2]. Therefore, it is essential to regulate the concentration of heavy metals in wastewaters before their disposal to the environment [3].

There exist a number of methods for removal heavy metals from aqueous systems. Chemical precipitation, ion exchange, adsorption, ultrafiltration, constructed wetland, and membrane

* Corresponding Author Email: *tegened@yahoo.com*

separation have been used for heavy metal removal. However, there are limitations in efficiency of the methods employed for the removal of heavy metals from wastewater before being discharged into the environment. Adsorption is the most commonly used technique for the removal of chromium from wastewater due to it is high removal efficiency, regeneration of adsorbent, low cost, ease of operation, and absence of secondary pollutant formation [4].

Among the commonly used adsorbents, bio-synthesized nanoparticles are the most prominent candidates because they are reproducible, non-toxic, environment-friendly, and low-cost adsorbents with relatively high adsorption capacity [5]. Recently, a number of researchers have reported synthesis of nanoparticles via a green method, for use as an effective adsorbent for heavy metal removal. Similarly synthesis of Fe_3O_4 MNPs via a green chemistry approach has been reported elsewhere. For instance, Fe_3O_4-NPs has been synthesized using brown seaweed aqueous extract containing sulfated polysaccharide as a reducing and stabilizing agent [6] and in another report fast, single-stage, and completely eco-friendly synthesis of iron oxide nanoparticles (Fe_3O_4–NPs) employing green synthesis via *P. pavonica* and *S. acinarium* plant part extract has been communicated. The report indicated that the nanoparticle had exhibited a high capacity for removal of Pb with value ranging from 78.6 - 91% after 75 min of contact time. The authors also reported that the iron oxide magnetic nanoparticles had efficiency to remove about 82% of Lead and 77% of Cadmium at initial concentration of 50 mg/l and pH 5 [7].

Various studies have witnessed that biomolecules like polyphenols, saponins, organic acids, vitamins, polysaccharides, and terpenoids play a great role in reducing and capping nanoparticles. Currently, there is an increasing demand to develop environmentally friendly nanoparticle synthetic processes that are free from toxic chemicals within the synthesis protocol. As a result, researchers dealing with synthesis and assembly of nanoparticles have shifted their approach towards methodologies employing biological systems [8].

Catha edulis (khat) is a plant grown commonly in the horn of Africa. The *Catha edulis* plant leaf extract contains phytochemicals such as alkaloids, cathine and dimer of cathinone, triterpenes, sterols, fatty alcohols, hydrocarbon carboxylic acid, and saponins. The alkaloids, cathinone, are presumably the main psychoactive components of Khat [9]. In this study the Khat leaf extract was chosen due to the fact that the plant is locally available and contain chemical constituents that would act as reducing and capping agents.

The authors were motivated to undergo this study as there are few or no reports of researches related to the green synthesis of magnetite nanoparticles using *Catha edulis* plant leaf extract as capping and /or reducing agent. Similarly, its applications in wastewater treatment are rarely reported. Hence, this article presents the successful green synthesis of magnetite nanoparticles using *Catha edulis* plant leaf extract and evaluation of its efficiency for chromium (VI) removal from aqueous solutions.

MATERIALS AND METHODS

Apparatus and Instruments

The apparatus and equipment that were used during this research work were Uv-Vis spectrometer (T80$^+$- PG instrument), Diffuse reflectance spectroscopy (Uv-Vis DRS Elico SL-150 spectrophotometer), XRD (Shimadzu, XRD-7000S South Korea), FTIR (FTIR Perkin Elmer's spectrophotometer), SEM (Scanning Electron Microscopy), TGA (Thermogravimetric Analysis), electronic balance, oven, beaker, test tube, magnetic stirrer, thermometer, Whatman No.1, filter paper, measuring cylinder, pH-meter, spatula, Erlenmeyer flask, volumetric flask, the ceramic crucible, Buchner funnel, and bar magnet.

Chemicals and Reagents

The chemicals and reagents including Ferrous chloride tetrahydrate ($FeCl_2.4H_2O$, Sigma-Aldrich, 99% purity), Ferric chloride hexahydrate ($FeCl_3.6H_2O$, Sigma-Aldrich, 99% purity), Hydrochloric acid (HCl, Riedel dehaen,Germeny,37 % HCl), Sodium hydroxide (NaOH, Sigma- Aldrich 99% purity), Ethanol (C_2H_5OH 99.8%, Fmd, Ethiopia), Potassium dichromate ($K_2Cr_2O_7$, Sigma-Aldrich 99% purity), Sulfuric acid (H_2SO_4, Sigma-Aldrich 98% purity), 2,5 diphenylcarbazide were purchased from Loba Chemie Pvt Ltd and were used as received without further purification. Khat (*Catha edulis*) plant leaf was purchased from local market in Adama town, Ethiopia. All the chemicals used in this study were analytical grade.

Collection of Catha edulis (Khat) Plant Leaves

The Khat (*Catha edulis*) leaf samples obtained from local market were thoroughly washed several

Fig. 1. Steps involved in the preparation of *Catha edulis* plant leaf.

times with tap water followed by distilled water to remove extraneous matter. The cleaned Khat leaves were completely dried at room temperature in open air under shadow for 15 days to remove moisture content. The dried leaves of the *Catha edulis* plant were crushed by using an electrical grinding machine to produce a fine powder (Fig. 1).

Preparation of Catha edulis Plant Leaf Extract

The extraction of the plant leaf part was carried out by taking 3.0 g of the powdered leaves into a 500 mL round bottom flask followed by the addition of 100 mL of distilled water. Then the mixture was allowed to boil at 60°C for about 2 hours. The suspension formed in the solution was allowed to cool for about 15 minutes and was filtered twice by using Whatman's № 1 filter paper. Then the resulting plant extract was kept in refirgrator at 4°C for the synthesis of magnetite nanoparticles (Fig. 2).

Phytochemicals test of Catha edulis plant leaf extract

The presence of alkaloids, glycosides, flavonoids, phenols, saponins, steroids, and tannins (gelatin) in the *Catha edulis* plant leaf extract were examined according to reported procedure with minor modifications [9].

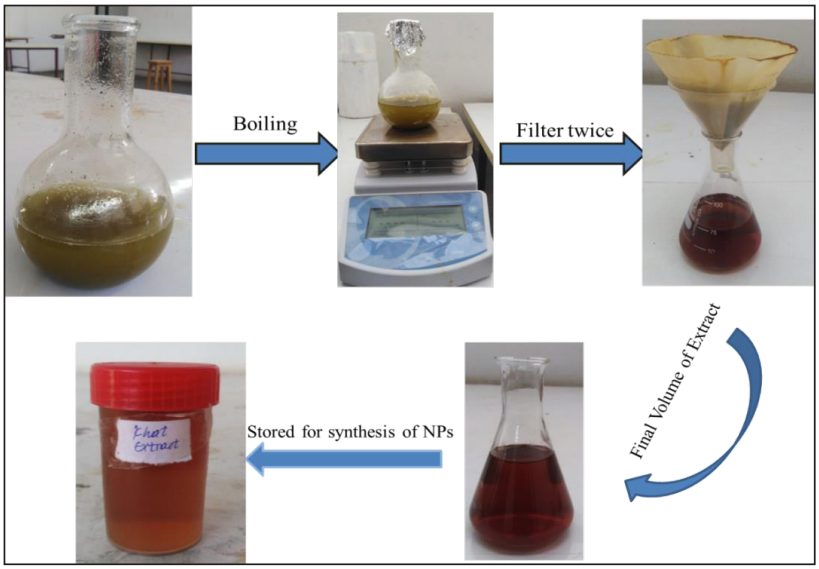

Fig. 2. Steps involved in the preparation of *Catha edulis* plant leaf extract.

Synthesis of magnetite NPs Using Khat (Catha edulis) Leaves Extract

The synthesis of magnetite (Fe_3O_4) was carried out by taking ferrous chloride and ferric chloride in 1:2 ratios respectively. Precisely, 2.65 g of ferrous chloride tetra hydrate ($FeCl_2{\cdot}4H_2O$) and 5.3 g of ferric chloride hexahydrate ($FeCl_3{\cdot}6H_2O$) were dissolved in 500 mL distilled water under mild magnetic stirring at 80 °C on a hot plate. After 15 min, light orange color appeared and different amounts of Catha edulis leaf extract were added while stirring on a hot plate. In a typical experiment, the extract was added to ferric chloride and ferrous chloride precursor solution in three different ratios by volume. In the first case (1:1 ratio); 50 mL of ferrous chloride tetrahydrate, Ferric chloride hexahydrate, and 50mL of *Catha edulis* leaf extract, the second case was for 1:2 ratio in which 33.3 mL of Ferrous chloride tetrahydrate, Ferric chloride hexahydrate and 66.7 mL of *Catha edulis* leaf extract were added and for third (2:1 ratio) case, 66.7 mL of Ferrous chloride tetrahydrate, Ferric chloride hexahydrate and 33.3 mL of *Catha edulis* leaf extract were added. In almost all the cases, the solution turned brownish-black from orange and after 5 min, 100 mL of 1 M NaOH was added, and black precipitates of magnetite (Fe_3O_4) were prepared. Then after 5 min of stirring, the solution was removed from the hot plate and left for settling down of iron oxide nanoparticles precipitates. Black precipitates of magnetite (Fe_3O_4) were washed five to eight times with distilled water and were dried in a hot air oven for 8 h at 80 °C. The prepared magnetite particles were stored in a tightly closed jar for characterization and further experimental use (Fig. 3) [10].

CHARACTERIZATION OF MAGNETITE NANOPARTICLES

Characterization using X-ray diffractometer (XRD)

To determine crystallinity, structure imperfections, and crystallite size of the synthesized Fe_3O_4 Nps XRD were examined by using the Shimadzu XRD-700 X-ray diffractometer (XRD. The x-ray diffraction (XRD) patterns were recorded at the range of 2θ from 10 to 80 with a scan rate of 20/ min using Cu Kα (λ = 1.5406 A^0) radiation with an accelerating voltage of 40 KV. The crystallite size D of a particle can be estimated according to the Scherrer equation (eqn. 1 below).

$$D = \frac{k\lambda}{\beta \cos\theta} \quad (1)$$

where, the x-ray wavelength λ is 0.154 nm, k is the structure factor, which is assigned a value of 0.94, D is the average diameter of the crystals, θ is the Bragg angle in degrees, and β is the full-width at half-height of the prominent peaks [26].

Characterization of Fe_3O_4 Nanoparticles Using Scanning Electron Microscope (SEM)

The morphological information and characteristics [11] of Fe_3O_4 nanoparticles were studied by SEM. SEM analysis of the biosynthesized Fe_3O_4 NPs was carried out by using SEM (JCM-6000 plus BENCH TOP SEM, SHIMADZU

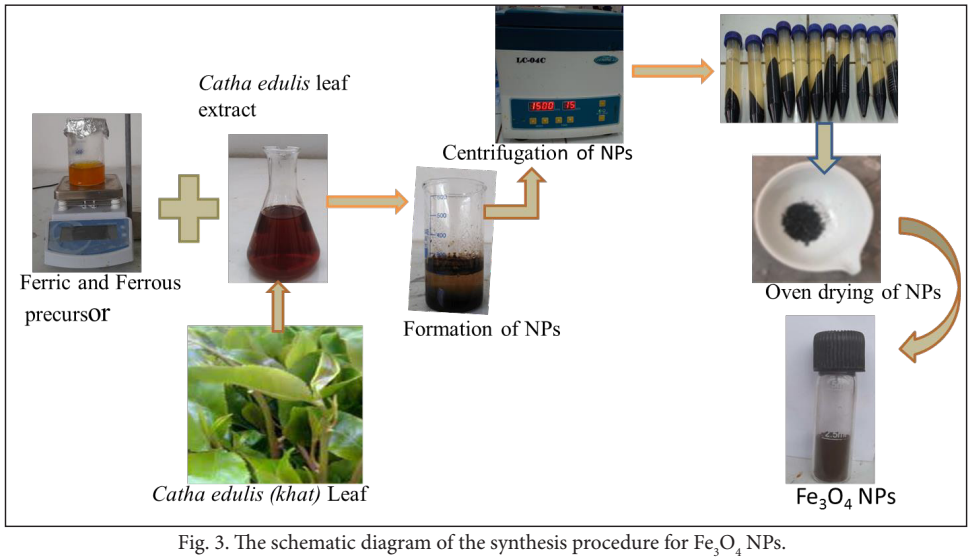

Fig. 3. The schematic diagram of the synthesis procedure for Fe_3O_4 NPs.

Corporation, Japan).

Characterization of Fe_3O_4 Nanoparticles Using Fourier Transform Infrared (FTIR)

FT-IR was used to identify the functional groups of the active components responsible for synthesizing Fe_3O_4 NP. FTIR spectrum of the dried powder of the biosynthesized Fe_3O_4 samples was recorded on 65 FT-IR (PerkinElmer) in the range 4000-400 cm^{-1} with a resolution of 2.0 cm^{-1} [12].

Characterization of Fe_3O_4 Nanoparticles Using UV-Vis Spectroscopy

The optical properties and band gap energy of biosynthesized magnetite nanoparticles were characterized by Uv-Vis DRS Elico SL-150 spectrophotometer The UV-Vis absorption analysis was carried out with spectral range of 200 nm to 800 nm.

Characterization of Fe_3O_4 Nanoparticles Using Thermogravimetric analysis (TGA)

Thermogravimetric analysis of the biosynthesized Fe_3O_4 nanoparticles was done at Bahirdar University Chemistry Department in a flowing air atmosphere and the thermograms were recorded in the temperature range of 25–800 ^{0}C, at a heating rate of 20 ^{0}C/min. TGA measures the percent weight loss of a test sample.

Stock solution preparation

The standard stock solution of chromium (1000 mg/L) was prepared by dissolving 2.828 g of 99.9 % analytical grade $K_2Cr_2O_7$ in 1000 mL of distilled water. Standard working solutions of chromium with different concentrations 20, 30, 40, 50 and 60 mg/L were prepared from the stock solution by appropriate dilutions. 1, 5-diphenylcarbazide was used for the spectrophotometric determination of Cr (VI). The pH of the aqueous solution was adjusted to by the addition of 0.1 M HCl or 0.1M NaOH solution [13].

Batch adsorption experiments

Batch adsorption experiments were carried out at constant temperature T= 25± 2^{0}C by varying adsorbent dose (250mg – 1250mg), Cr (VI) ion concentration (20–60 mg L^{-1}), agitation time (30min - 120 min), and pH values (3, 5, 7, 9, 11). The solutions of Cr (VI) comprised of potassium dichromate ($K_2Cr_2O_7$) were taken into Erlenmeyer flasks. After pH was adjusted, a known quantity of adsorbent was added and finally metal-bearing suspensions were kept under magnetic stirring. The suspension obtained after shaking was allowed to settle using an external magnet and the residual adsorbent was filtered using Whatman № 1 filter paper, and metal ion concentrations in the filtrate were determined by UV-VIS spectrophotometer.

The percentage removal of Cr(VI) ion and adsorption capacity was computed using reported equations 2 and 3, respectively [14].

$$\text{Chromium removal (\%)} = \frac{(Co - Ce)}{Co} x\ 100 \quad (2)$$

$$\text{Adsorption capacity } (q_e) = \frac{(Co - Ce)V}{M} \quad (3)$$

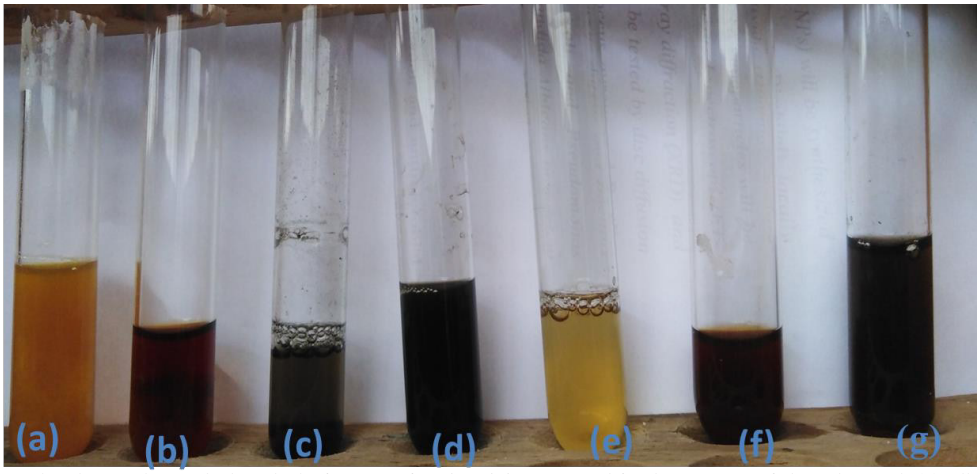

Fig. 4. The color change observed when the leaf extract of *Catha edulis* was tested for the presence of phytochemicals (a) Alkaloids, (b) Glycosides, (c) flavonoids, (d) Polyphenols, (e) saponins, (f) steroids, and (g). Tannins.

Where C_0 is the initial chromium (VI) ion concentration, C_e is the chromium (VI) ion concentration at equilibrium, V is the volume of the solution, m is the mass of the adsorbent, and q_e is the adsorption capacity.

Adsorption Kinetics Study

Adsorption kinetics was used to understand absorption mechanisms and the effect of contact time on adsorption. In each sample of 20, 30, 40, 50, and 60mg/L solution of hexavalent chromium, 1 g of magnetite was added while stirring at 100 rpm at pH of 6-10. Samples were taken at 20 min, 40 min, 60 min, 80 min, and 100 min time intervals. Finally, the samples were filtered to remove magnetite particles and then diluted for adsorption measurements [15]

Adsorption isotherm of hexavalent chromium on magnetite

Equilibrium isotherms were obtained as follows. Several solutions with different known hexavalent chromium concentrations (20, 30, 40, 50, and 60 mg/L) were prepared and transferred to separate beakers. During continuous mixing on the stirring rod, 1g/L of magnetite was added to each sample. After stirring for 10 min the beakers were placed for 120 min to settle magnetite nanoparticles. Samples were taken from the upper clear part of the solution then diluted and equilibrium concentrations were measured using cuvette tests.

RESULTS AND DISCUSSION

Phytochemicals Screening Test of Catha edulis plant leaf extract

Phytochemicals screening is important as it gives information about the classes of compounds present in plant materials that might serve in reducing, capping, and stabilizing the nanoparticles. For instance, biomolecules such as proteins, phenols, and flavonoids play a great role in reducing the ions to nanosize and also play an important role in the capping of NPs. The results of analysis of the phytochemicals present in *Catha edulis* plant extract employed for the green synthetic procedures in our study clearly indicated that secondary metabolites such as flavonoids, glycosides, polyphenols, tannins, saponins and alkaloids as shown in Figs**.** 4(a-g) were among the major constituent of the plant extract.

The color change formed during phytochemicals investigation serves as indicator of the formation of different complexes as a result of oxidation and reduction reactions. For example, the yellow color of the alkaloid indicates that the nitrogen or oxygen atom of the amide groups of the alkaloids involve in a reaction. In most of the ferric chloride tests, the iron (III) ion forms complexes having different colors depending on the nature of the complexes [9].

This indicates that *Catha edulis* plant leaf extract contains phytochemicals which are capable of reducing the iron oxide by donating electrons, capping, and stabilizing it during the synthesis of the magnetite nanoparticles. [16].

Characterization of Synthesized Fe_3O_4 NPs

Physical property analysis

The light yellow color of $FeCl_2.4H_2O$ and $FeCl_3.6H_2O$ solutions (Fig. 5(a)) were changed to light orange color upon string on the hot plate and also this light orange color started changing to

Fig. 5. Colors of precursors and green synthesized NPS a) ferrous and ferric chloride precursor, (b) leaf extract of *Catha edulis* and (c) Fe_3O_4NPs.

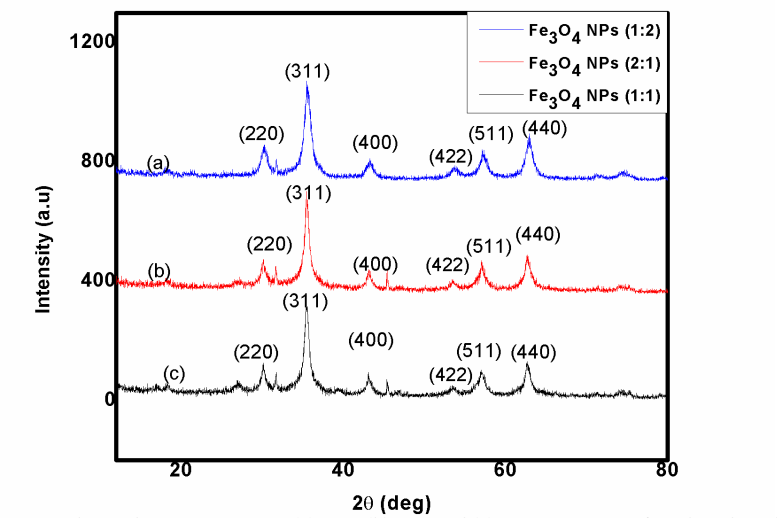

Fig. 6. XRD patterns of green synthesized Fe_3O_4 NPs using: (a) 1 : 1, (b) 2 : 1 and (c) 1 : 2 mass ratio of $FeCl_3$ and $FeCl_2$ to plant extract.

brownish-black as shown in Fig. 5(c) as soon as *Catha edulis* plant leaf extract (Fig. 5(b)) was added to iron salt precursor solution. These color changes indicate that the reduction is spontaneous for the formation of magnetite nanoparticles.

The brownish-black color observed could be the result of the interaction between the Iron ion in the precursor solution and biomolecules that are present in *khat* leaf extract [17], which led to the spontaneous reduction process. The biomolecules present in *Catha edulis* plant leaf extract consist of a phenolic ring and various electron-donating groups such as –OH, C=O, -OOH, etc. Electron conjunction resonance and tautomerism are known to increase in the availability of electrons for reduction to occur. In addition after sharing electron, the electron-donating group forms a covalent bond with iron nanoparticles which prevent agglomerations of particle and impart stability to green synthesized magnetite nanoparticle.

X-ray Diffraction (XRD) Analysis

The XRD analysis provides information about the phase purity and crystallinity of nanoparticles. In this study, the three samples synthesized by varying metals to plant extract ratios i.e., (1:2), (2:1), and (1:1) showed similar in the peak position and intensity distribution in the XRD pattern

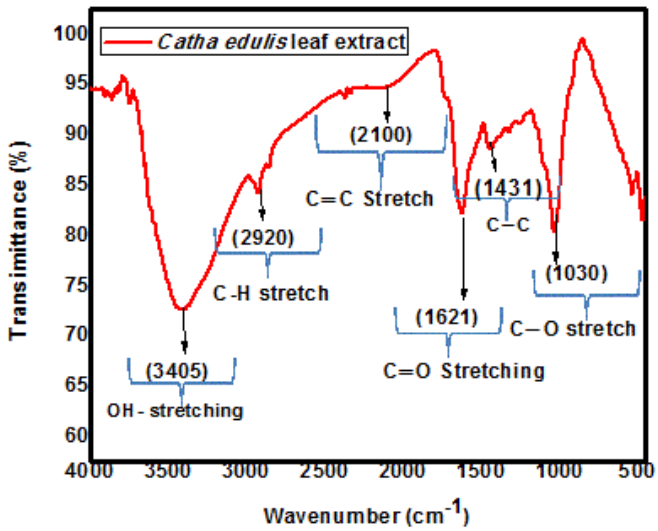

Fig. 7. FTIR spectrum of *Catha edulis* plant leaf extract.

(Fig. 6). the diffraction peak was observed for 1:2 ratio at 2θ = 30.23°, 35.45°, 43.27°, 53.7°, 57.1°, and 62.1°, which are corresponds to the crystal plane of (220), (311), (400), (422), (511) and (440) (Fig. 6a). For the 2:1 ratio, diffraction peaks found at 2θ values around 30.1°, 35.45°, 43.00°, 53.4°, 57.1°, and 62.7° were assigned to crystal planes of (220), (311), (400), (422), (511) and (440) (Fig. 6b). Similarly, for metal to plant extract ratio of 1:1 (Fig. 6c), the diffraction peaks were observed at 2θ values of 30.23°, 35.4°, 43.1°, 53.4°, 57.0°, and 62.6°, corresponds to a crystal plane of (220), (311), (400), (422), (511) and (440).

The diffraction peak of Fe_3O_4NPs was found to be in good agreement with JCPDS card number 00-019-0629, which confirms the formation of pure Fe_3O_4 NPs. The green synthesized Fe_3O_4 nanoparticle possessed higher crystallinity, and no XRD detectable impurities were observed in these samples as well, which confirms the purity of the magnetite (Fe_3O_4) nanoparticle [17].

The crystal size of the green synthesized magnetite (Fe_3O_4) nanoparticle was also calculated using the Debye Scherer equation [18]. Accordingly, considering the highest intense peaks, the crystal size were calculated and found to be 12.13 nm, 14.06 nm, and 9 nm for 1:1, 2:1, and 1:2, metal to plant extract ratios respectively. It was also observed that the size of the NPs decrease with increasing the amount of the plant extract which hinders the agglomeration of the nanoparticles. This result confirmed that the *Catha Edulis* plant extract was responsible for the reduction or capping of the nanoparticle

Fourier Transform Infrared (FTIR) Analysis

FTIR tests were done to determine the potential biomolecules responsible for the reduction, capping, and effective stabilization of the green synthsised nanoparticles [19]. The FTIR spectra of *Catha edulis* plant leaf extract are presented in Fig. 7. The strong absorption peak of *Catha edulis* plant leaf extract observed at 3405 cm^{-1} indicates the –OH vibrational stretching of alcohol and phenolic compounds. A band at 2920 cm^{-1} reveals the C-H stretching of hydrocarbon. The peak at 2100 cm^{-1} was due to stretching vibration of alkenes or aromatic C=C bending. The peaks at 1431 and 1030 cm^{-1} corresponded to C-C weak stretching vibration of Alkane and C-O stretching bond. The existence of these biologically active plant compounds might have been accountable for the reducing and capping of magnetite (Fe_3O_4) NPs. The phytochemicals with the aforementioned functional groups exhibit capping and reduction nature of *Catha edulis* plant extract on the surface of nanomaterials. These results were in good agreement with previous reports related to the synthesis of magnetite (Fe_3O_4) NPs using different plant extracts [20,21].

The FTIR spectrum of green synthesized magnetite nanoparticles before and after adsorption is presented in Fig. 8. The spectral peaks at 3393 cm^{-1} and 3284 cm^{-1} could be assigned to the O-H stretch of alcohol and phenol moieties. A band at 1569 cm^{-1} and 1600 cm^{-1} revealed the presence

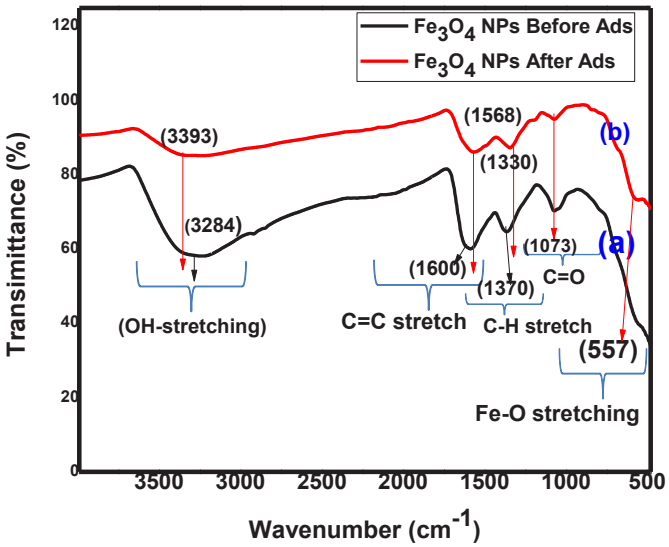

Fig. 8. FTIR spectrum of green synthesized magnetite (Fe_3O_4) nanoparticles a) before adsorption and b) after adsorption.

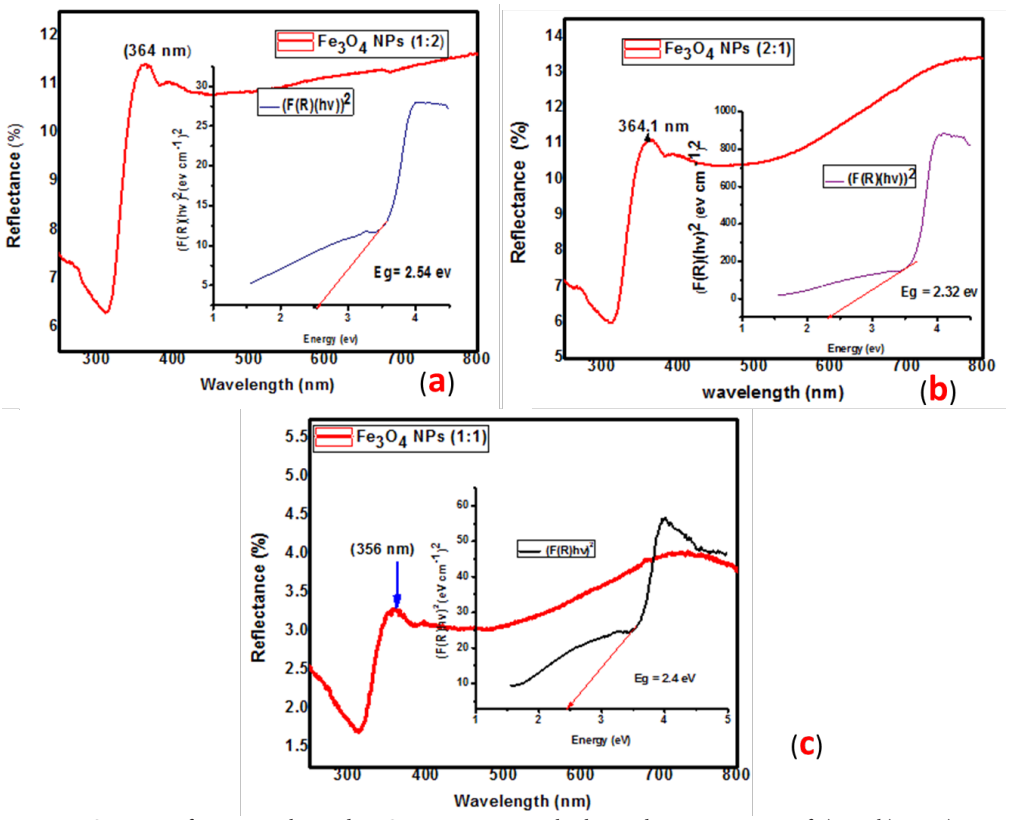

Fig. 9. Uv-Vis DRS spectra of green-synthesized Fe_3O_4 NPs using metal salts to plant extract ratio of a) 1:2, b) 2:1, c) 1:1 and their corresponding band gap energy.

of C=C of the carbonyl group (1550-1650) [22] and the stretching vibrations of amides were also appear in this range [23]. A band at 1330 cm^{-1} and 1370 cm^{-1} refers to the C-H stretching of an alky group. Peaks at 1073 cm^{-1} represent the stretching vibration of the carboxylate group (C=O, whereas the peak observed around 1073 cm^{-1} might be due to stretching vibration of the C-OH bond from proteins in the plant extract [24]. The absorption band at 557 cm^{-1} corresponds to characteristic Fe-O bond which further confirms the interaction of the phytochemicals with the nanoparticle [25].

The absence of additional peaks in the FTIR spectrum of nanoparticles Figs. 8(a-b) after adsorption have been has been confirmed. In fact, any chemical bond between chromium anions and nanoparticles has not been formed during the adsorption process. Thus, the adsorption process of Cr(VI) onto Fe_3O_4 nanoparticles could be suggested to proceed through phsysisorption. This phemnomenon may facilitate the reuse of magnetite nanoparticles as recycleable adsorbents in wastewater treatment procedures [22].

UV-Vis DRS Analysis of Fe_3O_4 NPs

The optical property and band gap energy of the green synthesized magnetite nanoparticle was analyzed by using diffuse reflectance spectroscopic measurement (Fig. 9). The UV-Vis spectrum of the magnetite nanoparticles revealed the success of the reduction process and formation of nanoparticles. The formation of the magnetite nanoparticle was confirmed by the immediate change in color of the reaction mixture from light yellow to dark brown after the addition of *Catha edulis* plant leaf extract. The physical change in color observed during the synthesis process was supported by the spectral data obtained from the UV-Vis analysis in which a strong peak in the range of 355–365 nm for each of the three-various ratios of Fe_3O_4 NPs synthesized has appeared.

The band gap energy (Eg) of magnetite nanoparticles was calculated using Kubelka–Munk model. This model can be expressed using equation 4 below.

$$F(R) = (1-R)^2/2R \quad (4)$$

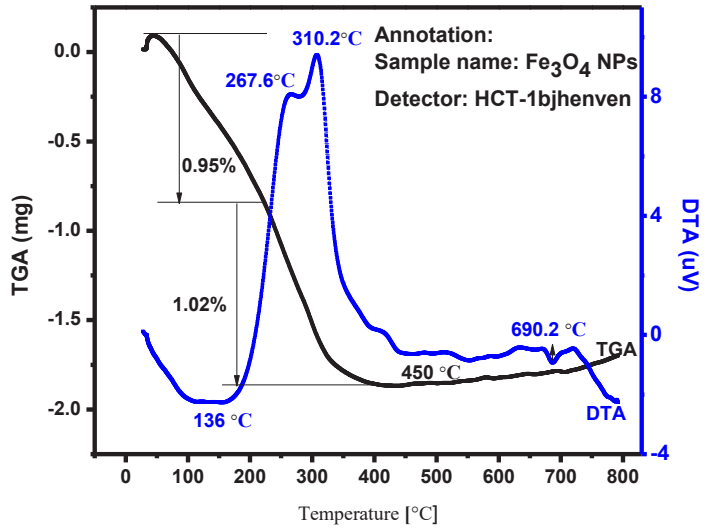

Fig. 10. The TGA-DTA plots of green synthesized magnetite (Fe_3O_4) NPs.

Where F(R) is the Kubelka-Munk function, and R is the reflectance. The band gap represents the minimum energy necessary to excite an electron up to a state in the conduction band to take part in conduction [26].

The band gap energies of the nanoparticles were found to vary with varying the ratios of the metal salt to plant extract. Accordingly, the calculated band gaps were 54 eV (Fig. 9(a)), 2.32 eV (Fig. 9(b)), and 2.4 eV (Fig. 9(c)) for Fe_3O_4 (1:2), Fe_3O_4 (2:1), and Fe_3O_4 (1:1) nanoparticles respectively. The result corroborates that the Fe_3O_4 NPs formed by the use of higher volume of the plant extract, exhibited larger band gap energy and this indicates that the energy band gap of Fe_3O_4NP is associated with particle size. The smaller the particle size the larger the band gap. This phenomenon can be explained quantum mechanically as the particle size reaches the nanoscale, the number of overlapping orbitals or energy levels decreases, and the thickness of the band becomes thinner. This in turn causes a rise in the energy band gap between the valence band and the conduction band [27]. Furthermore, this band gap value agrees with the fact that Fe_3O_4 which is an n- and p-type semiconductor has low resistivity owing to its minor bandgap in the range of 0.1–3 eV [28].

Thermogravimetric analysis of biosynthesized Fe_3O_4 NPs

The TGA analysis was done to study the thermal stability, decomposition temperature, and also decomposition rate of the synthesized nanoparticles. The TGA curve of Fe_3O_4 NPs is shown in Fig. 10**.** The TGA plot reveals three weight loss steps in the tested temperature range which are associated with degradation of the main component of the nanoparticle. The first weight loss of about 0.95% happened at 180 °C and one exothermic peak of the DTA curve at 136 °C; indicating the removal of H_2O and organic moieties. In the second stage, two endothermic peaks observed at 267.6°C, 310.2°C, and 1.02% weight loss depicts the decomposition of the biomolecules from the plant extract. The temperature above which the weight loss became constant was used as the calcination temperature for the synthesized Fe_3O_4 nanoparticles. In the last step, there were no weight losses throughout the range of 450– 800°C, and exothermic peaks are observed in the DTA curve at 690.2°C. Hence, calcination of the magnetite nanoparticle was performed at 450 °C to remove unwanted plant extract residues and improve the purity of the nanoparticle [29].

SEM analysis of biosynthesized Fe_3O_4 NPs

The surface morphology of the green-synthesized Fe_3O_4 NPs adsorbent was characterized by using scanning electron microscope (SEM). The SEM image (Fig. 11) of the adsorbent material was recorded before and after adsorption of Cr (VI) metal ions on the surface. The data revealed that Fe_3O_4 NPs exhibited different morphologies and microstructural characteristics.

The structure and morphology of Fe_3O_4 NPs adsorbent before adsorption Fig. 11(a) showed

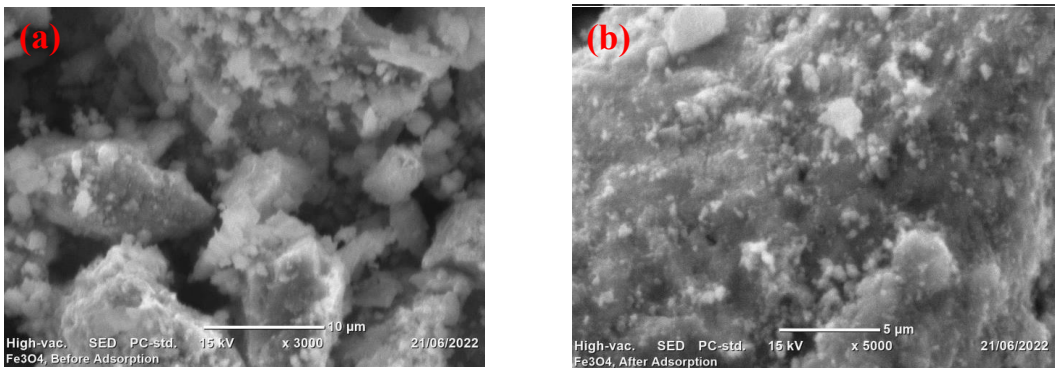

Fig. 11. SEM images of: (a) Fe_3O_4 NPs before adsorption (b) Fe_3O_4 NPs after adsorption.

vacant pores of various size and shape on the adsorbent. However, after the adsorption of Cr (VI) as shown in Fig. 11(b), the Fe_3O_4 NPs surface showed a reduction in the size of some pores, disappearance in some cases, disappearance of corners or edges, corrosion, and roughening. This confirmed that the pores of the adsorbent were filled with the hexavalent chromium ion and the surface has become puffy due to the resulting heterogeneity.

Batch Adsorption Studies

Calibration curve for standard solution were done by various concentrations (10 mg/L, 20 mg/L, 30mg/L, 40mg/L). The experiments were repeated three times and the average data were used to plot the resultant graphs. A calibration curve of absorbance against chromium concentrations was plotted as seen in Fig. 12. The experimental data reported in the following figure were fitted by a straight line with a high correlation coefficient value (R^2= 0.99986).

Optimization Design of Different Parameters

The optimization of parameters was done considering different ratios of nanoparticle to determine the nanoparticle that could have the maximum chromium removal efficiency. At initial concentration of 20 mg/L, maximum removal of 97.2% (1:1 Fe_3O_4 NPs), 96.9 % (2:1 Fe_3O_4 NPs) and 98.2% (1:2 Fe_3O_4 NPs) of chromium were achieved with three ratio of Fe_3O_4 NPs by keeping other parameters constant (pH =5, adsorbent dosage =1000 mg, contact time = 90 min). It was observed from the previous XRD analysis that the particle size was found to be smaller in the case of 1:2 ratio. Hence, all the parameter optimization designs for the adsorption process study were done using this sample of Fe_3O_4 NPs for removal of Cr (VI).

Factors Affecting the Adsorption

Effect of pH on Adsorption

The pH of the aqueous solution is one of the important factors that controlled the adsorption process. The experiments of this stage were performed under the conditions of constant contact time (60 min), adsorbent dose (1000 mg), initial chromium concentration (20 mg/L), and various pH values from 3 to 11 were selected for the experimentation. The pH of the solution was regulated by using 0.1 M HCl or 0.1 M NaOH solutions and the chromium removal was investigated. The experimental result shown in Fig. 13(a) revealed that the removal efficiency of adsorbent Fe_3O_4 NPs was increased from pH 3 to 5 Fe_3O_4 NPs exhibited the highest percent removal (98.6%) of chromium (VI) at a pH value of 5 and by increasing pH, a drastic decrease in adsorption percentage was observed. This might be due to the weakening of the electrostatic force of attraction between the oppositely charged adsorbate and adsorbent ultimately leading to the reduction in sorption capacity [30].

Effect of Adsorbent Dosage

The effect of adsorbent dosage on the removal of Cr (VI) ion from the standard working solution of Cr (VI) concentration was studied. Fig. 13 (b) revealed that the percentage removal of Cr (VI) ion was increased from 75.4 % to 98.6 % as the amount of adsorbent dosage was also increased from 250 mg to 1250 mg. This result could mainly explain the influence of available adsorption sites on removal efficiency as increasing the adsorbent dose was found to increase the number of the active site available for adsorption. An increase in adsorption with dose can be attributed to increased surface

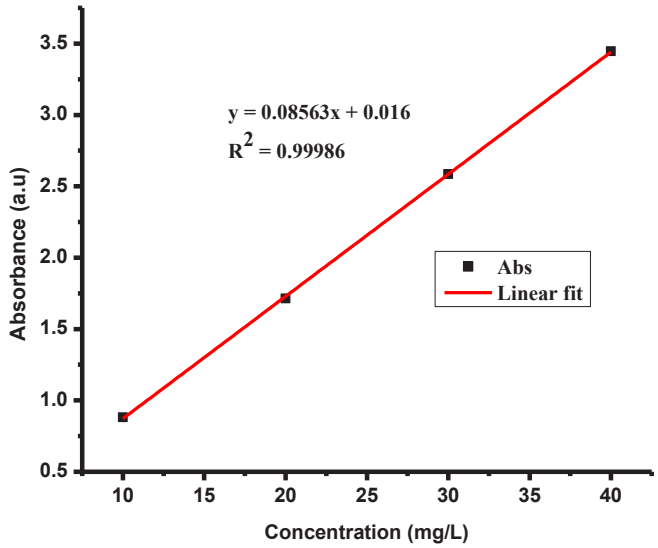

Fig. 12. Calibration curve for standards samples.

area and the availability of more binding sites for adsorption [31].

Effect of Contact Time

The Cr(VI) adsorption experiments were carried out for different contact times with fixed adsorbent dose, pH, and initial concentration. The effect of contact time on the adsorption efficiency of the Fe_3O_4 NPs with 20 mg/L of hexavalent chromium ion concentrations, pH=5, 1000 mg adsorption dose, and contact time (20 min,40 min,60 min,80 min, and 100 min). The chromium ion removal efficiency of the adsorbent has increased in the beginning but it decreased after reaching the equilibrium [32]. As shown in Fig. 13(c) the optimum contact time for adsorption of Cr (VI) ion by using Fe_3O_4 NPs was 60 minutes with a percentage removal of 96.1%. It is easy for chromium to access the active adsorption site, thus resulting in a rapid uptake of chromium. However, with an increase in contact time, the system attains a steady state. The occupancy of other remaining vacant sites becomes limited because of the repulsive force between chromium ion adsorbed on the surface and adsorbate in the solution [33].

Effect of Initial Concentration on Adsorption of Chromium

The effect of different initial chromium concentrations (20, 30, 40, 50, and 60 mg·L^{-1}) on the removal efficiency of chromium was studied, by keeping all the other parameters constant (at pH =5, contact time = 90 min, and absorbent dosage =1000 mg. as shown in Fig. 13(d) the chromium adsorption capacity was decreased from 98.6% to 64.8% with an increase in the initial concentration of Cr (VI) from 20mg/L to 60mg/L. On the other hand, the removal efficiency of Cr (VI) is higher at lower Cr (VI) concentrations with further residual Cr (VI) ions remaining in the aqueous solution [34]. This can be explained by the fact that all the adsorbents had a limited number of active sites, which would have become saturated above a certain concentration. For instance, a decrease in the percentage of removal with increasing initial concentration of chromium ion in this study is that as the ratio of chromium ion to Fe_3O_4 NPs increases, the exchangeable sites in Fe_3O_4 NPs structure are saturated, resulting in a decrease of the removal percentage.

Adsorption kinetics Study

An adsorption kinetics study is an important tool for analyzing the adsorption process of Cr (VI) on the surface of Fe_3O_4 nanoparticles was conducted using two common kinetic models pseudo-first-order (Eqn. 5) and pseudo-second-order (Eqn. 6).

$$\ln (q_e - q_t) = lnq_e - K_1 \text{ x } t \quad (5)$$

Where qe (mg/g) and qt (mg/g) are the mass of metal ion adsorbed at equilibrium and at time t, respectively. K_1 is the first-order rate constant

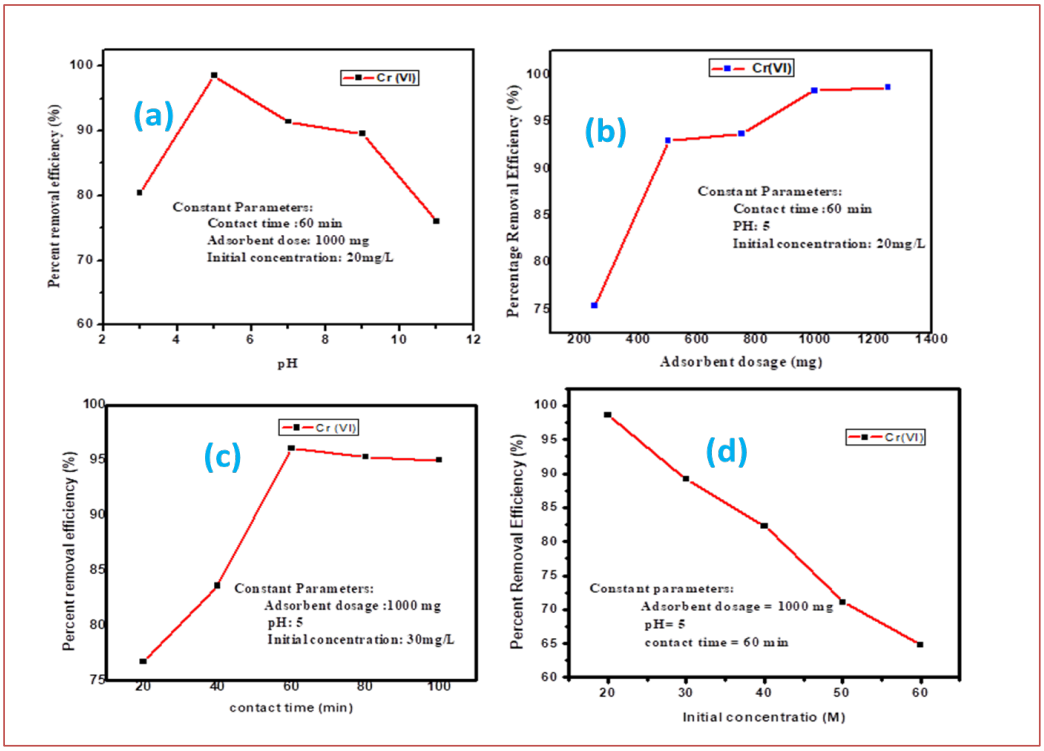

Fig. 13. Effect of pH (a) adsorbent dosage (b), contact time (c) and initial concentration (d) on the Cr ion adsorption by magnetite nanoparticles.

of adsorption. A straight line of log (q_e-q_t) versus t suggests the applicability of this kinetic model (Fig. 14). the values of q_e and K_1 were determined from the intercept and slope of the plot, to be .9474 and -0.00022 respectively (Table 1). The pseudo-first order kinetic model's poor correlation coefficient values suggest that adsorption does not take place solely on one site per ion.

$$\frac{1}{qt} = \frac{1}{k2\ qe^2} + \frac{1}{qe * t} \qquad (6)$$

Where, q_t is the metal uptake per unit weight of adsorbent (mg/g) at time t, qe is the metal uptake per unit weight of adsorbent (mg/g) at equilibrium, and k_2 (g/mg.min) is the rate constants of pseudo-second-order kinetics equations. The value of qe(mg/g) and K2 (g/mg min) were obtained from the slope and intercept of the plot of t/qt vs t described and were found to be 10.67773 and 6.19778 respectively (Fig. 15). Therefore, the result of the kinetic model study revealed that the adsorption process was best fitted to pseudo-second-order model which implied that the Cr (VI) adsorption on Fe_3O_4 NPs proceeded through chemical sorption (chemisorption) and the sorption capacity was proportional to the number of active sites on the sorbent [35]. Furthermore the pseudo second-order adsorption model is based on the assumption that the rate-controlling step of adsorption involved covalent bond through sharing or exchange of electrons between adsorbent and adsorbate, which means the rate depends on

Table 1. Adsorption kinetics constants at the same concentrations.

Metal ions	Pseudo 1st order kinetic model				Pseudo 2nd order kinetic model			
Cr (VI)	qe(mg/g)	qe_1	k_1	R^2	qe(mg/g)	qe_2	K_2	R^2
	1.20462	3.9474	-0.00022	0.67866	3.25849	10.67773	6.19778	0.98188

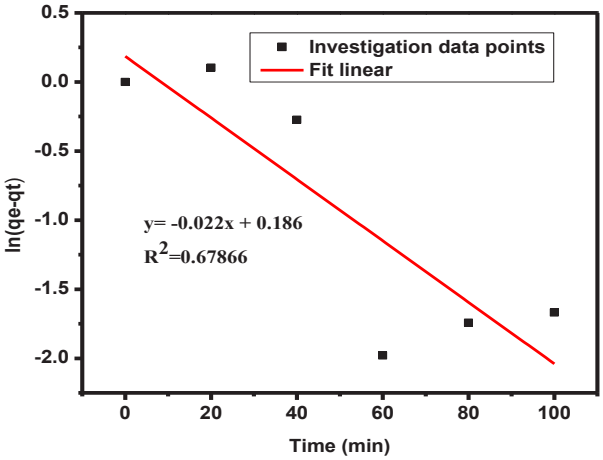

Fig. 14. Pseudo first-order adsorption kinetics of Cr(VI) on magnetite nanoparticles with the same concentrations.

concentrations of Fe_3O_4 NPs and the hexavalent chromium metal [36].

Adsorption Isotherm Study

Adsorption isotherms often describe the distribution of metal ions between the liquid phase and the solid phase, based on a set of assumptions that are mainly related to the heterogeneity/ homogeneity of adsorbents, the type of coverage, and the possibility of interaction between the adsorbate species. The most widely used isotherm equations are Langmuir and Freundlich's isotherm models.

Langmuir Isotherm Model

The Langmuir model assumes that the uptake of metal ions occurs on a homogenous surface by monolayer adsorption without any interaction between adsorbed ions. The Langmuir isotherm is represented by equation 7.

$$\frac{C_e}{q_e} = \frac{K_L C_e}{Q_m} + \frac{1}{Q_m} \quad (7)$$

where Ce (mg/l) is the concentration of adsorbate left in solution at equilibrium, K_L is the Langmuir binding energy, Qm(mg g^{-1}) is the adsorption maximum (mg g^{-1}) and qe(mg g^{-1}) is the amount of adsorbate adsorbed per unit mass of adsorbent. As shown in Fig. 16, however, the lower correlation coefficient obtained from the Langmuir plot (R^2 = 0.83304) for Cr(VI) compared to the Freundlich plot (R^2 = 0.98341) for Cr(VI), confirmed that the adsorption was not monolayer coverage of the surface of the magnetite

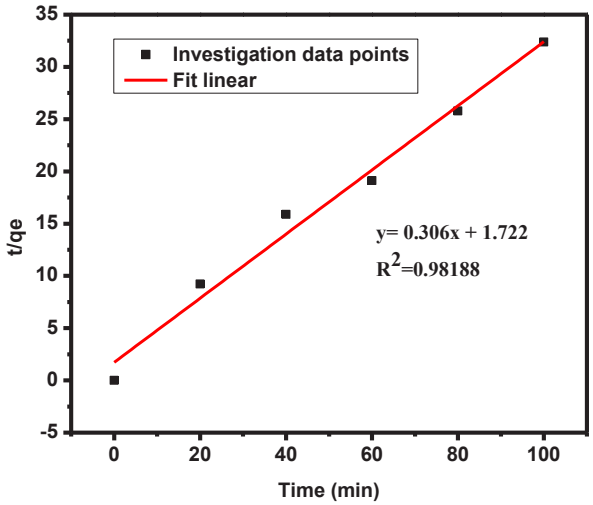

Fig. 15. Pseudo-second order adsorption kinetics of Cr (VI) on magnetite nanoparticles with the same concentrations.

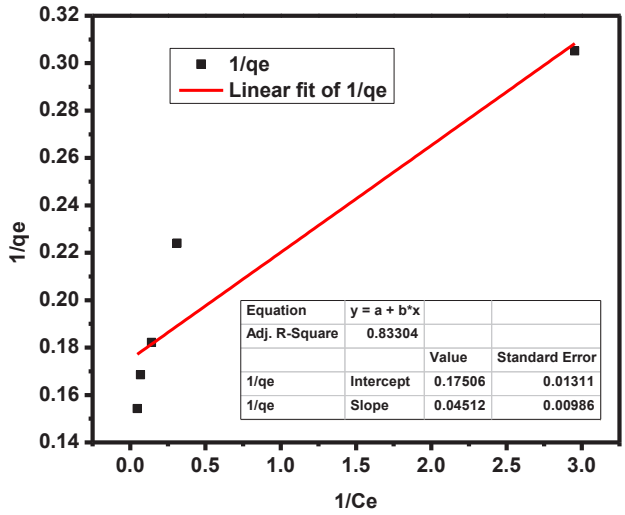

Fig. 16. Langmuir isotherm model for Cr (VI) adsorption.

nanoparticle by the Cr(VI).

Freundlich Isotherm Model

The monolayer adsorption of metal ions on a heterogeneous surface is what the Freundlich model predicts will happen [31]. Adsorption activities that take place on heterogeneous surfaces are subject to Freundlich isotherm. An expression for the surface heterogeneity and the exponential distribution of active sites and their energy could be provided by this isotherm [37]. The suitability of the isotherm was verified via the equation (8)

$$\text{Log } q_e = \log K_f + \frac{1}{n} \log C_e \qquad (8)$$

Where q_e denotes the quantity of adsorbed Cr (VI) per quantity of adsorbent at the conditions of equilibrium (mg/g), Ce denotes the equilibrium concentration (mg/L), and K_f denotes the capacity of adsorption, and n denotes the intensity of adsorption.

The results of the isotherm study presented in Fig. 16 and Fig. 17 indicated that the Freundlich model ($R^2 = 0.9834$) was better suited to adequately represent the examined sorption phenomenon than the Langmuir model ($R^2 = 0.83304$) (Table 2 and 3). Thus, it is suggested that multilayer adsorption of Cr(VI) occurred on the heterogeneous surface of the magnetite nanoparticle [38].

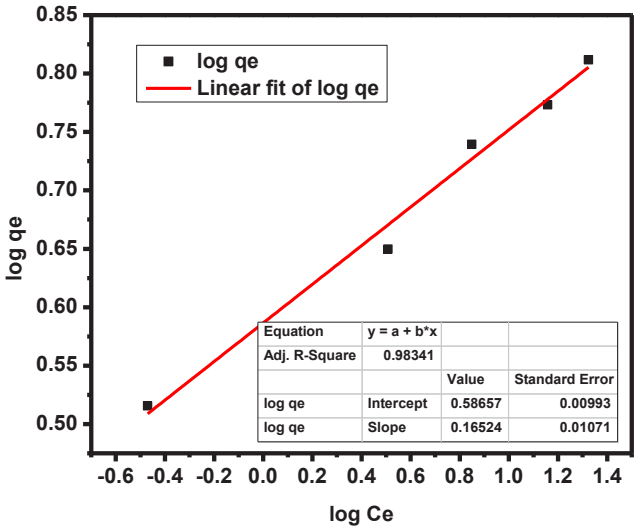

Fig. 17. Freundlich isotherm model for Cr (VI) adsorption.

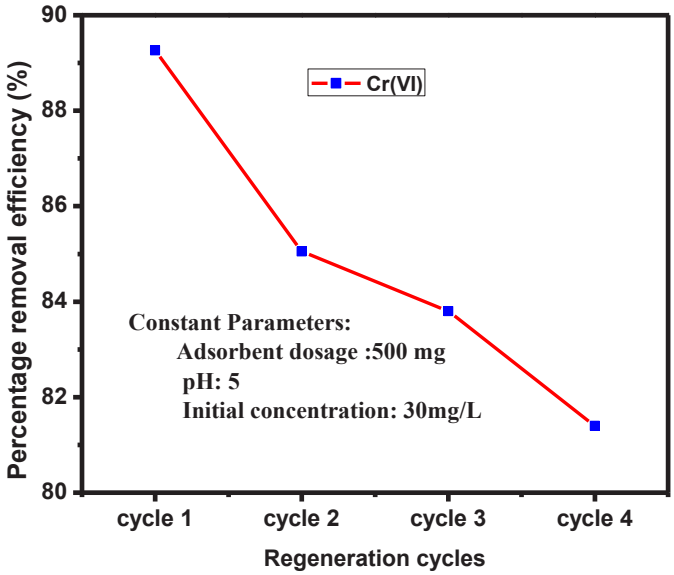

Fig. 18. Adsorbent regeneration experiment.

Desorption Study

Desorption studies were conducted to investigate the recyclability and reuseability of adsorbent material. Adsorbent reusability was checked by conducting four adsorption-desorption Cycles. The recycled Fe_3O_4 NP has been tested against the removal of Cr(VI) metal ions for the 1st, 2nd, 3rd, and 4th cycles, respectively and the data presented in Fig. 18. The regeneration cycles of the magnetic nanomaterial showed a slight decrease (about 7.86 % for Cr (VI) ions) in the removal efficiency between the 1st cycle and 4th cycle, indicating that the nanomaterial could be reused for up to 4 cycles sequentially without significant reduction in removal efficiency of Fe_3O_4 NPs against Cr (VI) metal ions.

CONCLUSION

In this study, green synthesis of magnetite nanoparticles using *Catha edulis* plant leaf extract as a reducing and capping agent was successfully carried out and the resulting nanoparticles were characterized using various techniques such as XRD, Uv-Vis, FTIR, SEM. In addition, the efficiency of the nanoparticles for Cr (VI) ion removal from an aqueous solution was investigated. The XRD study showed that the Fe_3O_4 NPs were cubic face-centered with an average crystallite size between 9 and 12 nm. FTIR studies have confirmed the reduction of Fe_3O_4 NPs by active metabolites found in plant leaf extract and the formation of the nanoparticle by the green synthesis method. UV-Vis DRS spectral data showed that the formation of magnetite nanoparticles had promoted the adsorption in a visible region of the spectra. The SEM image proved that Fe_3O_4 NPs exhibited different morphologies and microstructural characteristics. A batch adsorption experiment was used to investigate the efficiency of adsorbent by varying parameters such as pH, initial concentration; adsorbent dose and contact time at room temperature. The optimum adsorption of hexavalent chromium ion by Fe_3O_4 NPs was achieved at pH 5, adsorbent dose 1000mg, initial concentration 20 (mg/L), and contact time 60 min. The adsorption process was well described by the Freundlich adsorption isotherm. Pseudo-

Table 2. Langmuir isotherm model constants and correlation coefficients for adsorption of chromium.

Langmuir isotherms of Cr (VI)						
Estimated isotherm parameters	Intercept	Slope	qmax (mg/g)	KL	RL	R2
	0.58657	0.16524	1.704826	3.549806	178.4903	0.83304

Table 3. Freundlich isotherm model constants and correlation coefficients for adsorption of chromium.

Freundlich isotherms of Cr (VI)					
Estimated isotherm parameters	Intercept	Slope	1/n	K_f	R^2
	0.58657	0.16524	0.16524	3.859846	0.98341

second order kinetic model was best fitted to show the adsorption kinetics. The synthesized Fe_3O_4 NPs have exhibited nearly 98.6 % hexavalent chromium removal efficiency. In comparison with other nanoparticle, Fe_3O_4 NPs have high adsorption efficiency which could be attributed to the relatively high surface area, high reactivity, catalytic efficiency, and its superparamagnetic properties. Hence, the study confirmed that magnetite nanoparticle could find a potential application in heavy metal removal from aqueous solutions.

ACKNOWLEDGMENTS

The authors would like to thank Adama Science and Technology University for provison of materials and facilities to support this research work.

CONFLICT OF INTEREST

The authors declare no conflict of interest.

REFERENCES

1. Rajput S., Pittman C. U., Mohan D., (2016), Magnetic magnetite (Fe_3O_4) nanoparticle synthesis and applications for lead (Pb^{2+}) and chromium (Cr^{6+}) removal from water. *J. Colloid Interf. Sci*. 468: 334–346.
2. Dhal B., Abhilash A., Pandey B. D., (2018), Mechanism elucidation and adsorbent characterization for removal of Cr(VI) by native fungal adsorbent. *Sustain. Environ. Res.* 28: 289–297.
3. Weijiang Z., Yace Z., Yuvaraja G., Jiao X., (2017), Adsorption of Pb(II) ions from aqueous environment using eco-friendly chitosan schiff's base@Fe_3O_4 (CSB@Fe_3O_4) as an adsorbent; kinetics, isotherm and thermodynamic studies. *Int. J. Biol. Macromol.* 105: 422-430.
4. Jadidi M., Etesami N., Esfahany M. N., (2017), Adsorption and desorption processes of chromium ions using magnetic Iron Oxide nanoparticles and their relevant mechanism. *Iran. J. Chem. Eng.* 14: 31–40.
5. Michael S., Solomon K., Omoniyi A., (2020), Short review article plant-mediated Iron nanoparticles and their applications as adsorbents for water treatment – A review. *J. Chem. Rev.* 2: 103–113.
6. El-Kassas H. Y., Aly-Eldeen M. A., Gharib S. M., (2016), Green synthesis of iron oxide (Fe_3O_4) nanoparticles using two selected brown seaweeds: Characterization and application for lead bioremediation. *Acta Oceanol. Sin.* 35: 89–98.
7. Arjaghi S. K., Alasl M. K., Sajjadi N., Fataei E., Rajaei G. E., (2021), Green synthesis of Iron Oxide nanoparticles by RS lichen extract and its application in removing heavy metals of Lead and Cadmium. *Biol. Trace Elem. Res.* 199:763–768.
8. Bolade O. P., Williams A. B., Benson N. U., (2020), Green synthesis of iron-based nanomaterials for environmental remediation: A review. *Environ. Nanotechnol. Monit. Manag.* 13: 45-48.
9. Gebremedhn K., Kahsay M. H., Aklilu M., (2019), Green synthesis of CuO nanoparticles using Leaf extract of *Catha edulis* and its antibacterial activity. *J. Pharm. Pharmacol.* 7: 6-12.
10. Altaf S., Zafar R., Zaman W. Q., Ahmad S., Yaqoob K., Syed A., Khan A. J., Bilal M., Arshad M., (2021), Removal of levofloxacin from aqueous solution by green synthesized magnetite (Fe_3O_4) nanoparticles using *Moringa olifera*: Kinetics and reaction mechanism analysis. *Ecotoxicol. Environ. Saf*. 226: 112826.
11. Khoobi A., Salavati-niasari M., (2019), High performance of electrocatalytic oxidation in direct glucose fuel cell using molybdate nanostructures synthesized by microwave-assisted method. *Energy Elsevier.* 178: 50–56.
12. Khoobi A., Shahdost-fard F., Arbabi M., Akbari M., Mirzaei H., (2020), Sonochemical synthesis of $ErVO_4$/$MnWO_4$ heterostructures : Application as a novel nanostructured surface for electrochemical determination of tyrosine in biological samples. *Polyhedron*. 17: 114302.
13. Berihun D., (2017), Removal of Chromium from industrial wastewater by adsorption using coffee husk. *J. Mater. Sci. Eng.* 6: 1000331.
14. Singh R., Bhateria R., (2020), Optimization and experimental design of the Pb^{2+} adsorption process on a nano-Fe_3O_4-based adsorbent using the response surface methodology. *ACS Omega*. 5: 28305–28318.
15. Pandey P. K., Sharma S. K., Sambi S. S., (2010), Kinetics and equilibrium study of chromium adsorption on zeolite NaX. *Int. J. Environ. Sci. Technol*. 7: 395–404.
16. Andualem W. W., Sabir F. K., Mohammed E. T., Belay H. H., Gonfa B. A., (2020), Synthesis of copper oxide nanoparticles using plant leaf extract of *catha edulis* and its antibacterial activity. *J. Nanotechnol*. 2020: 1-10.
17. Dhar P. K., Saha P., Hasan M. K., Amin M. K., Haque M. R., (2021), Green synthesis of magnetite nanoparticles using Lathyrus sativus peel extract and evaluation of their catalytic activity. *Clean. Eng. Technol*. 3: 100117.
18. Basavaiah K., Kahsay M. H., Rama Devi D., (2018), Green synthesis of magnetite nanoparticles using aqueous pod extract of Dolichos lablab L for an efficient adsorption of crystal violet. *Emerg. Mater. Res*. 1: 121–132.
19. Sadeghi B., Rostami A., Momeni S., (2015), Facile green synthesis of silver nanoparticles using seed aqueous extract of *Pistacia atlantica* and its antibacterial activity.

Spectrochim. Acta Part A: Mol. Biomol. Spec. 134: 326–332.
20. Yew Y. P., Shameli K., Miyake M., Kuwano N., Bt Ahmad Khairudin N. B., Bt Mohamad S. E., Lee K. X., (2016), Green synthesis of magnetite (Fe_3O_4) nanoparticles using seaweed (*Kappaphycus alvarezii*). *Nanoscale Res. Lett*. 11: 276.
21. Gabal R. A., Shokeir D., Orabi A., (2022), Cytotoxicity and hemostatic one step green synthesis of Iron nanoparticles coated with green tea for biomedical application. *Trends Sci.*19: 3.
22. Jadidi M., Etesami N., Esfahany M. N., (2017), Adsorption and desorption processes of chromium ions using magnetic Iron Oxide nanoparticles and their relevant mechanism. *Iran. J. Chem. Eng.*14: 31–40.
23. Sadeghi B., Gholamhoseinpoor F., (2015), A study on the stability and green synthesis of silver nanoparticles using *Ziziphora tenuior* (Zt) extract at room temperature. *Spectrochim. Acta Part A: Mol. Biomol. Spect*. 134: 310–315.
24. Sadeghi B., Mohammadzadeh M., Babakhani B., (2015), Green synthesis of gold nanoparticles using *Stevia rebaudiana* leaf extracts: Characterization and their stability. *J. Photochem. Photobiol: Biology.* 148: 101–106.
25. Han C., Zhu D., Wu H., Li Y., Cheng L., Hu K., (2016), TEA controllable preparation of magnetite nanoparticles (Fe_3O_4 NPs) with excellent magnetic properties. *J. Magn. Magn. Mat*. 408: 213–216.
26. Gabal R. A., Shokeir D., Orabi A., (2022), Cytotoxicity and hemostatic one step green synthesis of Iron nanoparticles coated with green tea for biomedical application. *J. Trends Sci.* 19: 2062-2066.
27. Singh M., Goyal M., Devlal K., (2018), Size and shape effects on the band gap of semiconductor compound nanomaterials. *J. Taibah Univ. Sci*. 12: 470–475.
28. Yusefi M., Shameli K., Hedayatnasab Z., Yeang S., (2021), Green synthesis of Fe_3O_4 nanoparticles for hyperthermia, magnetic resonance imaging and 5-fluorouracil carrier in potential colorectal cancer treatment. *Res. Chem. Intermed.* 47: 1789–1808.
29. Geneti S. T., Mekonnen G. A., Murthy H. C. A., Mohammed E. T., Ravikumar C. R., Gonfa B. A., Sabir F. K., (2022), Biogenic synthesis of magnetite nanoparticles using leaf extract of *Thymus schimperi* and their application for monocomponent removal of chromium and mercury ions from aqueous solution. *J. Nanomater.* 2022: 1-15.
30. Nameni M., Alavi Moghadam M. R., Arami M., (2008), Adsorption of hexavalent chromium from aqueous solutions by wheat bran. *Int. J. Environ. Sci. Technol.* 5: 161–168.
31. Edris J., Gupta N., Zereffa E. A., (2019), Synthesis of silica supported Iron Oxide nanoparticles for hexavalent Chromium removal from aqueous solutions. *Ethiop. J. Sci. Sustain. Dev.* 6: 81–93.
32. Saravanan A., Kumar P. S., Govarthanan M., George C. S., Vaishnavi S., Moulishwaran B., Kumar S. P., Jeevanantham S., Yaashikaa P., (2021), Adsorption characteristics of magnetic nanoparticles coated mixed fungal biomass for toxic Cr(VI) ions in aquatic environment. *Chemosphere.* 267: 129226.
33. Kumar R., Bishnoi N. R., Garima A., Bishnoi K., (2008), Biosorption of chromium(VI) from aqueous solution and electroplating wastewater using fungal biomass. *J. Chem. Eng*. 135: 202–208.
34. Ataabadi M., Hoodaji M., Tahmourespour A., Kalbasi M., Abdouss M., (2014), Optimization of factors affecting hexavalent chromium removal from simulated electroplating wastewater by synthesized magnetite nanoparticles. *Environ. Monit. Assess.* 187: 4165, PMID: 25471623.
35. Marcu C., Varodi C., Balla A., (2021), Adsorption kinetics of chromium (VI) from aqueous solution using an anion exchange resin solution using an anion exchange resin. *Anal. Lett*. 54: 140-149.
36. Hong J., Xie J., Mirshahghassemi S., Lead J., (2020), Metal (Cd, Cr, Ni, Pb) removal from environmentally relevant waters using polyvinylpyrrolidone-coated magnetite nanoparticles. *RSC Adv*. 10: 3266–3276.
37. Ayawei N., Ebelegi A. N., Wankasi D., (2017), Modelling and interpretation of adsorption isotherms. *J. Chem*. 2017: 1–11.
38. Zubair Y. O., Fuchida S., Tokoro C., (2020), Insight into the mechanism of arsenic(III/V) uptake on mesoporous zerovalent Iron–magnetite nanocomposites: Adsorption and microscopic studies. *ACS Appl. Mater. Interf*. 12: 49755–49767.